Quantifying the impact of synoptic circulation patterns on ozone variability in North China from April-October 2013-2017

Jingda Liu[1,2], Lili Wang[2,4], Mingge Li[2,5], Zhiheng Liao[6], Yang Sun[2], Tao Song[2], Wenkang Gao[2], Yonghong Wang[4], Yan Li[7], Dongsheng Ji[2], Bo Hu[2], Veli-Matti Kerminen[4], Yuesi Wang[1,2,3,5], Markku Kulmala[4]

[1]Department of Atmospheric Physics, Nanjing University of Information Science & Technology, Nanjing 210044, China

[2]State Key Laboratory of Atmospheric Boundary Layer Physics and Atmospheric Chemistry (LAPC), Institute of Atmospheric Physics, Chinese Academy of Sciences, Beijing 100029, China

[3]Centre for Excellence in Atmospheric Urban Environment, Institute of Urban Environment, Chinese Academy of Science, Xiamen, Fujian 361021, China

[4]Institute for Atmospheric and Earth System Research / Physics, Faculty of Science, University of Helsinki, Finland

[5]University of Chinese Academy of Sciences, Beijing 100049, China

[6]School of Atmospheric Sciences, Sun Yat-sen University, Guangzhou, Guangdong, China

[7]Fangshan Meteorological Bureau, Beijing, 102488, China

Correspondence to: Lili Wang (wll@mail.iap.ac.cn)

Abstract

The characteristics of ozone variations and the impacts of synoptic and local meteorological factors in North China were quantitively analyzed during the warm season from 2013 to 2017 based on multicity in situ ozone and meteorological data as well as meteorological reanalysis. The domain-averaged maximum daily 8-h running average O_3 (MDA8 O_3) concentration was 122±11 μg m^{-3}, with an increase rate of 7.88 μg m^{-3} $year^{-1}$, and the three most polluted months were closely related to the variations in the synoptic circulation patterns, which occurred in June (149 μg m^{-3}), May (138 μg m^{-3}) and July (132 μg m^{-3}). Twenty-six weather types (merged into 5 weather categories) were objectively identified using the Lamb-Jenkinson method. The highly-polluted weather categories included S-W-N directions (geostrophic wind direction diverts from south to north), low-pressure related weather types (LP) and cyclone type, which the study area controlled by low-pressure center (C), and the corresponding domain-averaged MDA8 O_3 concentrations were 122, 126 and 128 μg m^{-3}, respectively. Based on the frequency and intensity changes of the synoptic circulation patterns, 39.2% of the interannual increase in the domain-averaged O_3 from 2013 to 2017 was attributed to synoptic changes, and the intensity of the synoptic circulation patterns was the dominant factor. Using synoptic classification and local meteorological factors, the segmented synoptic-regression approach was established to evaluate and forecasted daily ozone variability on an urban scale. The results showed that this method is practical in most cities, and the dominant factors are the maximum temperature, southerly winds, relative humidity on the previous day and on the same day, and total cloud cover. Overall, 41-63% of the day-to-day variability in the MDA8 O_3 concentrations was due to local meteorological variations in most cities over North China, except for two cities: QHD (Qinhuangdao) at 34% and ZZ (Zhengzhou) at 20%. Our

quantitative exploration of the influence of both synoptic and local meteorological factors on interannual and day-to-day ozone variability will provide a scientific basis for evaluating emission reduction measures that have been implemented by the national and local governments to mitigate air pollution in North China.

1 Introduction

Tropospheric ozone (O_3) is one of the air pollutants of greatest concern due to its considerable harm to human health and vegetation (Kinney, 2008; Fleming et al., 2018; Mills et al., 2018). O_3 is formed through nonlinear interactions between NO_x and volatile organic compounds in combination with sunlight (Monks et al., 2009; Monks et al., 2015). Thus, ozone levels are controlled by precursors and meteorological conditions. With industrialization advancement and rapid economic growth, North China has become one of the most populated and polluted regions in the world. The national and local governments have implemented a series of measures to reduce emissions since 2013, and although $PM_{2.5}$ has decreased significantly, O_3 pollution is still severe in this region (Lu et al., 2018; Li et al., 2019). Several studies have explored the variation in summer ozone in China (He et al., 2017; Liao et al., 2017; Lu et al., 2018; Li et al., 2019). However, systematic research aimed at quantifying the evolution of ozone and meteorological impacts and contributions throughout the warm season (April-October) was limited during the five years (2013-2017) when the Action Plan for Air Pollution Prevention and Control (www.gov.cn/zwgk/2013-09/12/content_2486773.htm) was implemented. This lack of analysis has prevented a clear understanding of the effect of emission reduction measures on ozone in North China from being obtained.

Meteorological factors affect ozone levels through a series of complex combinations of processes, including emissions, transport, chemical transformations and removal (Chan and Yao, 2008; Jacob and Winner, 2009; Lu et al., 2019). Meteorological conditions are the primary factor that determine the day-to-day variations in pollutant concentrations over China (He et al., 2016; He et al., 2017), whereas long-term O_3 trends are influenced both by climatological (weather types, temperature, humidity, and radiation, etc.) and environmental factors (changes in anthropogenic and natural sources). Therefore, the impact of reduced anthropogenic emissions on O_3 variations can be estimated more accurately if we are able to quantify the meteorological influence.

Synoptic meteorological conditions have an important effect on regional ozone distribution and variation (Shen et al., 2015). A given synoptic circulation pattern represents a particular range of meteorological conditions; therefore, synoptic classification is a useful method for gaining insight into the impact of meteorology on ozone levels at regional scale. Previous studies have demonstrated a significant connection between the weather type and surface O_3 concentration; however, the relation between these two quantities varies in different regions due to differences in the topography, pollution source, local circulation, etc.(Moody et al., 1998; Cooper et al., 2001; Hegarty et al., 2007; Demuzere et al., 2009; Monks et al., 2009; Wang et al., 2009a; Zhang et al., 2012; Zhang et al., 2013; Pope et al., 2016; Liao et al., 2017). For example, based on the Lamb-Jenkinson weather typing technique, Demuzere et al. (2009) demonstrated increased surface O_3 concentrations in summer in an easterly weather type at a rural site in Cabauw, Netherlands, whereas the opposite result was obtained by Liao et al. (2017) in the Yangtze River Delta region in eastern China. Therefore, synoptic classification and its relationship with O_3 need to be explored separately in different regions. In addition, based on synoptic classification, Comrie and Yarnal (1992) and Hegarty et al. (2007) suggested a reconstructed pollutant concentration

(caused by synoptic influence) algorithm, which can separate the climatological and environmental variability in environmental data. It was found that 46% and 50% of the interannual variability in the O_3 concentration was reproduced in the northeastern United States (Hegarty et al., 2007) and Hong Kong (Zhang et al., 2013), respectively, by taking into account the interannual changes in the frequency and intensity of synoptic patterns.

At the urban scale, the daily variation in the ozone concentration is affected by both synoptic and local meteorological factors. Quantifying the contribution of local meteorological factors to day-to-day variations in ozone concentrations will provide a scientific basis and guidance for reasonable ozone reduction measures, and clarifying and quantifying the relationship between meteorological factors and ozone concentration is vital for daily forecasts of ozone pollution potential. Weather type classification prior to regression analysis is superior to a simple linear regression approach (Eder et al., 1994; Barrero et al., 2006; Demuzere et al., 2009; Demuzere and van Lipzig, 2010), and synoptic-regression-based algorithm can reproduce the observed O_3 distributions and provide a better parameterization to promote the understanding of the dependence of ozone on meteorological factors in a given urban region.

Overall, in this study, we explore how the maximum daily 8-h running average O_3 (MDA8 O_3) concentration varies and quantify the contributions of synoptic and local meteorological conditions to the ozone variability in North China (58 cities covering Hebei, Shanxi, Shandong, and Henan Provinces and Beijing and Tianjin municipalities) during April-October in 2013-2017. Our specific goals are to 1) demonstrate the characteristics and variation trends in the surface MDA8 O_3 concentration; 2) classify the predominant weather types and meteorological mechanisms underlying the regional ozone levels and variability; 3) quantify the contributions of changes in synoptic circulation patterns (frequency and intensity) to the interannual variability in the O_3 concentration; and 4) quantify the contributions of local meteorological factors to day-to-day variations in O_3 levels, and identify the prominent meteorological variables and construct O_3 potential forecast model for major cities..

2 Data and methods

2.1 Ozone and $PM_{2.5}$ data

The hourly O_3 and $PM_{2.5}$ data during April-October, 2013-2017 were derived from the National Urban Air Quality Real-time Publishing Platform (http://106.37.208.233:20035/). According to technical regulation for ambient air quality assessment (HJ 663-2013, http://www.mee.gov.cn/), the MDA8 O_3 concentration was calculated for each monitoring site based on the hourly data from the time period 08:00-24:00 for the days with at least 14 hours of measurement data. If less than 14 hours of valid data are available, the results are still valid if the MDA8 O_3 concentration exceeds the national concentration limit standard. Each city has at least two monitoring sites, and the MDA8 O_3 levels for a city are the corresponding averages over all sites in that city. The MDA8 O_3 values were collected in only 14 cities for the time period from 2013-2017 and in an additional 44 cities for the time period from 2015-2017, and the detailed information is shown in Fig. 1 and Table S1. The original units for the ozone observations was $\mu g\ m^{-3}$, and the conversion coefficient from the mixing ratios (unit: ppbv) to $\mu g\ m^{-3}$ was a constant (e.g., 0.5 at a temperature of 25 °C and pressure of 1013.25 hPa). In this study, we used the original units. Unless otherwise noted, the analysis of O_3 refers to MDA8 O_3 during April-October in this paper.

2.2 Meteorological data

Gridded-mean sea level pressure data, 10-meter U and V wind components (U_{10} and V_{10}, respectively), boundary layer height (BLH) and 2-meter temperature (T_2) with a 1° horizontal resolution and vertical velocity (ω) from 1000-100 hPa (27 levels) and wind divergence (div) from 1000-850 hPa (7 levels) in 6-h intervals (Beijing time 02, 08, 14 and 20) for 2013-2017 were obtained from the European Center for Medium Weather Forecast Reanalysis Interim (ERA-Interim).

Four measurements per day for temperature (T), relative humidity (RH), total cloud cover (TCC), rain, wind speed (ws), wind direction (wd), and pressure (pre) in 58 cities during April-October 2013-2017 were obtained from the China Meteorological Administration in the Meteorological Information Combine Analysis and Process System (MICAPS). Then, daily mean meteorological factors were averaged from four measurements (scalar averaging for most factors and vector averaging for wind speed and wind direction, which involved using the u (U) and v (V) components for averaging). The meteorological station with a minimum distance from the city center was chosen.

2.3 Lamb-Jenkinson circulation typing

The Lamb-Jenkinson weather type approach (Lamb, 1972; Yarnal, 1993; Conway and Jones, 1998; Trigo and Dacamara, 2000; Mckendry et al., 2006; Demuzere et al., 2009; Russo et al., 2014; Santurtún et al., 2015; Pope et al., 2016; Liao et al., 2017) has been widely employed to classify synoptic circulation. On the basis of the Lamb-Jenkinson method, the weather type circulation pattern for a given day is described using the locations of the high- and low-pressure centers that identify the direction of the geostrophic flow; the method uses coarsely-gridded pressure data on a 16-point moveable grid (Demuzere et al., 2009). In our study, North China was set as the center. The specific schematic diagram is shown in Fig. 1a. The daily mean sea level pressure data were averaged over four time points to determine the daily weather type. The detailed classification procedure can be found in Trigo and Dacamara (2000) and in the supplementary information (Text S1).

2.4 Reconstruction of O_3 concentration based on weather types

To quantify the interannual variability captured by the variations in the surface circulation pattern, Comrie and Yarnal (1992) suggested an algorithm to separate synoptic and non-synoptic variability in environmental data; by multiplying the overall mean value of a particular pattern by the occurrence frequency of that type of year, the climate signal can be obtained as follows:

$$\overline{\overline{O_{3\,m}}}(\mathrm{fre}) = \sum_{k=1}^{26} \overline{O_{3k}} F_{km} \qquad (1)$$

where $\overline{\overline{O_{3\,m}}}(\mathrm{fre})$ is the reconstructed mean MDA8 O_3 concentration influenced by the frequency of changes in the weather type from April-October for the year m, $\overline{O_{3k}}$ is the 5-year mean MDA8 O_3 concentration for weather type k, and F_{km} is the occurrence frequency of weather type k during April-October for year m.

Hegarty et al. (2007) suggested that variations in the circulation patterns are attributed to not only frequency changes but also intensity variations; moreover, they noted that the environmental and climate-related contributions to the interannual variations in ozone could be better separated by considering these two changes. As a result, Equation (1) was modified into the following form:

$$\overline{\overline{O_{3\,m}}}(\mathrm{fre+int}) = \sum_{k=1}^{26} (\overline{O_{3k}} + \Delta O_{3km}) F_{km} \qquad (2)$$

where $\overline{\overline{O_{3\,m}}}(fre + int)$ is the reconstructed mean MDA8 O_3 concentration influenced by the frequency and intensity of the changes in circulation patterns from April-October for year m; ΔO_{3km} is the modified difference on the fitting line, which is obtained through a linear fitting of the annual MDA8 O_3 concentration anomalies (ΔO_3) to the circulation intensity index (CII) for circulation pattern k in year m. ΔO_{3km} represents the part of the annual observed ozone oscillation caused by the intensity in each circulation pattern. Hegarty et al. (2007) used the domain-averaged sea level pressure (mslp) to represent the CII.

To better characterize intensity variations, we used addition 5 CIIs: the difference between the highest pressure and lowest pressure (gradient), the center pressure of the highest pressure system (max slp), the center pressure of the lowest pressure system (min slp), the distance from the highest pressure centers to the study city (dis max), and the distance from the lowest pressure centers to the study city (dis min). Among the above 6 CIIs, that having the strongest correlation coefficient (r) with ΔO_3 was selected as an effective circulation intensity index (ECII). Thus, ECII was used in Equation (2) to calculate ΔO_{3km}. All CIIs for the 14 cities were calculated based on 10°×10° grids covering North China (32°N-42°N, 110°E-120°E). An example of ΔO_{3km} (weather type C in ZJK which is a city located in Hebei province) is shown in Fig. 7a. Here, min slp has the highest r (-0.97) among the 6 CIIs in type C in ZJK, so min slp is selected as the ECII.

2.5 The segmented synoptic-regression approach and model validation

The utilization of a segmented synoptic-regression approach can aid in minimizing the errors when using linear regression to model a nonlinear relationship and effectively forecast ozone variations (Robeson and Steyn, 1990; Liu et al., 2007; Demuzere and van Lipzig, 2010; Liu et al., 2012). Based on locally monitored meteorological data, their 24-h time lag values and weather type classifications, stepwise linear regression was used in every weather category to construct the ozone potential forecast model. The details of the main methods are shown in Text S2. Notably, in this research, after excluding the missing data and disordering the time sequences, 80% of these days were used to build the potential forecast equations, and the remaining 20% were used to validate the accuracy of the equations.

Statistical model performances were evaluated according to the following factors: R^2 (variance in the individual model's coefficients of determination), RMSE (root mean square error), and CV (coefficient of variation defined as RMSE/mean MDA8 O_3). All statistics are based on MATLAB R2015b.

3. Results and discussion

3.1 Characteristics and variation trend of ozone concentrations in North China

The MDA8 O_3 concentration is one of six factors used to calculate the daily air-quality index in China. Five ranks were separated, representing different air-quality levels: excellent, good, lightly polluted, moderately polluted and heavily polluted days, with cut-off concentrations of 100, 160, 215 and 265 μg m^{-3}, respectively. The daily limit for the Grade II National Ambient Air Quality Standard is 160 μg m^{-3}. The spatial distribution of the averaged MDA8 O_3 concentration (Fig. 1b) and exceedance ratio, which represents the proportion of days exceeding the standard (160 μg m^{-3}) (Fig. 1c), as well as detailed information on the 58 cities (Table S1), showed a severe ozone pollution problem during the last five years in North China. The domain-averaged MDA8 O_3 concentration for 58 cities was 122±11 μg m^{-3}, with an increasing rate of 7.88 μg m^{-3} $year^{-1}$ and an exceedance ratio of 22.2±8.2%. Notably, the most

polluted cities were concentrated in Beijing, the southeast of Hebei and the west and north of Shandong, where the average MDA8 O_3 concentration was 130±9 μg m^{-3} and the exceedance ratio was 27.9±7.2%.

The daily evolution of MDA8 O_3 concentrations in 14 cities from 2013-2017 (Fig. 2a) indicated periodic, consistent and regional characteristics of ozone pollution. The most highly polluted periods were from mid-May to mid-July. In particular, the frequency and level of ozone pollution increased significantly in 2017, and the number of regionally persistent ozone pollution events increased. The rate of the increase in the MDA8 O_3 concentration from 2013-2017 was 0.87 μg m^{-3} $month^{-1}$ (Fig. 2b), and this growth was accompanied by a decrease in the $PM_{2.5}$ concentration (Fig. S1). A reduction in particle extinction due to a decreased $PM_{2.5}$ concentration can lead to an increase in radiation reaching the ground; in addition, Li et al. (2019) suggested that decreased $PM_{2.5}$ concentrations slowed the sinking of hydroperoxyl (HO_2) radicals and thus stimulated ozone production. Thus, the rise in ozone was partly due to the decline in $PM_{2.5}$. Overall, the annual domain-averaged MDA8 O_3 concentrations for 58 cities were 102, 109, 116, 119 and 136 μg m^{-3} in 2013, 2014, 2015, 2016 and 2017, respectively (Fig. 3a). The exceedance ratios for all cities were found to be 12.9%-19.4% from 2013 to 2016 but reached 31.1% in 2017.

The monthly-mean MDA8 O_3 concentrations (Fig. 3b) from April to October were 112, 138, 149, 132, 124, 117 and 75 μg m^{-3}, respectively, and the corresponding exceedance ratios were 9.4, 30.1, 41.1, 26.1, 20.3 20.1 and 3.3%. The highest domain-averaged MDA8 O_3 concentration and exceedance ratio occurred in June, followed by those in May, July, August, September, April and October. Meteorological conditions led to high ozone concentrations in June, and monsoon circulation in July and August resulted in cloudy, rainy conditions and less radiation in the study area (Wang et al., 2009c; Tang et al., 2012). The higher ozone concentrations in April than compared with those in October could be associated with strong winds, resulting in a downward transport of ozone due to the lower stratosphere folding mechanism (Stohl and Trickl, 1999; Cooper et al., 2002; Delcloo, 2008; Verstraeten et al., 2015). Notably, this conclusion is different from that of Tang et al. (2012), who reported that the ozone concentration in July was higher than that in May in North China during 2009-2010. However, as our study indicated that the domain-averaged MDA8 O_3 in May was even higher than that in July, the concentrated pollution episode occurred earlier, especially in 2017. The second half of May was the most polluted period, when the exceedance ratio was 46.1%, which is higher than the ratios observed in the first half of June (39.5%), the second half of June (45.4%) and the first half of July (35.6%). The reason for this difference is probably the abnormally high temperatures in May, especially the second half of May, from 2013-2017 and particularly in 2017 (Fig. S2). Many studies have found a strong positive correlation between ozone levels and temperature (Bloomer et al., 2009; Demuzere et al., 2009; Bloomer et al., 2010; Pusede et al., 2015).

3.2 Weather types and associated surface O_3 levels

3.2.1 The meteorological conditions and regional ozone concentrations under different predominant weather types

Based on the Lamb-Jenkinson weather typing technique, 26 circulation patterns affecting North China were identified, including two vorticity types (anticyclone, A, and cyclone, C), eight directional types (northeasterly, NE; easterly, E; southeasterly, SE; southerly, S; southwesterly, SW; westerly, W; northwesterly, NW; and northerly, N) and 16 hybrids of vorticity and directional types (CN, CNE, CE, CSE, CS, CSW, CW, CNW, AN, ANE, AE, ASE, AS, ASW, AW, and ANW). The composite mean sea

level pressure maps, along with the occurrence days, are shown in Fig. 4. There are distinctly different locations of the high-pressure and low-pressure centers under the different circulation conditions. The occurrence ratios of vorticity types, pure directional types, and hybrid types were 35.6%, 38.8% and 25.6%, respectively, during all 1070 days.

The mid-latitude eastern Eurasian continent is strongly affected by monsoon circulation, and there are several key synoptic systems affecting the circulation and meteorological conditions in North China. During our study period, North cyclones (Mongolian and Yellow River cyclones), which are indicative of a low-pressure system located in northwest North China, dominated in spring and summer. The Siberian High influenced northern China in spring and autumn. The Western Pacific Subtropical High was also a key system in summer. Therefore, these main synoptic systems resulted in variations in the frequencies of the various weather types in different months over North China.

According to the different locations of the different central systems, together with the similar meteorological factors and mean MDA8 O_3 values in these circulation patterns, 26 circulation types were merged into 5 weather categories: 1) N-E-S direction (geostrophic wind direction diverts from north to south) including N, NE, E, SE, AN, ANE, AE and ASE; 2) S-W-N direction (geostrophic wind direction diverts from south to north)including S, SW, W, NW, AS, ASW, AW and ANE; 3) LP (low-pressure related weather types) including CN, CNE, CE, CSE, CS, CSW, CW and CNW; 4) A (anticyclone); and 5) C (cyclone). The occurrence ratios of the 5 weather categories were 25.4%, 26.5%, 12.5%, 17.5% and 18.1% in all 1070 days. The predominant local meteorological conditions associated with a specific weather category play an important role in ozone pollution, influencing ozone photoreaction or its regional transport. The values of the averaged MDA8 O_3 concentration, frequency of weather types/categories and meteorological variables are depicted in Table 1 and Fig. 5. Briefly, the N-E-S direction and A categories were typically associated with cool and wet air, moderate rain and TCC, low BLH, and relatively clean air masses from the Inner Mongolia/eastern ocean region (Fig. S3); these conditions are unfavorable for ozone formation; thus, the corresponding area-averaged MDA8 O_3 concentrations were 98±6 μg m^{-3} and 96 μg m^{-3}, respectively. The S-W-N direction category had moderate T and BLH, low RH, weak wind, sporadic clouds and rain, and strong subsidence in the lower troposphere, which contributed to high ozone levels (122±8 μg m^{-3}). The highest ozone concentrations (126±16 and 128 μg m^{-3}) were related to the LP and C categories, which can probably be attributed to the meteorological conditions (hot and humid air, a small amount of TCC and rainfall, and high BLH) that were favorable for ozone formation and transport. However, CE and CSE were different from the other weather types in the LP category, with low O_3 concentrations due to low temperatures and easterly winds from the ocean. Overall, the peak values of ozone always occurred in the front of the passage of a cold front or cyclone (most weather types in LP and C), whereas the lowest values occurred during or after the passage of a cold front (most weather types in the N-E-S direction, C with heavy rainfall and CE); similar conclusions were also previously reported (Cooper et al., 2001; Cooper et al., 2002; Chen et al., 2008)

3.2.2 Spatial distributions of the 26 weather types/five categories

The spatial distribution of the averaged MDA8 O_3 concentration under different weather types is shown in Fig. 6, and Figs. S3-S7 display the spatial distributions of the combined wind field with BLH, maximum temperature (Tmax), RH, rain and TCC, respectively. In most cities, the lowest MDA8 O_3 concentrations occurred in the N-E-S direction and A weather categories. The S-W-N direction category, having predominantly southerly winds throughout the region or south of North China, exhibited high

ozone values along with the prevailing wind direction. The LP and C weather categories, having the highest regional averaged levels, were associated with high Tmax and strong southerly flow, moderate RH and ample sunshine, which are the meteorological conditions that are favorable for ozone formation as well as the transport of ozone and its precursors from polluted areas.

3.2.3 Interannual/monthly ozone variation elaborated from the perspective of circulation pattern changes

The interannual or monthly ozone concentration changes are associated with variations in weather types. Fig. 3 indicates that the ratios of high-ozone weather categories (S-W-N direction, LP and C S-W-N direction, LP and C) were most frequent in 2013 and 2017, less frequent in 2015 and 2016, and least frequent in 2014. The high-ozone weather categories accounted for 61.5% and 61.8% of the time in 2013 and 2017, respectively. Under similar weather conditions, low ozone levels could also be associated with high $PM_{2.5}$ levels in 2013 and 2015. The contributions of frequency-only and circulation changes (frequency and intensity) to the interannual ozone variability will be discussed in Section 3.3.

Due to the impacts by monsoon circulation systems, the frequencies of weather types varied dramatically on a monthly scale (Fig. 3b). The frequencies of both the N-E-S direction and A gradually decreased in spring, whereas the frequencies of the S-W-N direction, LP and C gradually increased. In autumn, the frequencies of LP and C decreased, whereas those of the S-W-N direction, N-E-S direction and A increased. The weather categories C and LP dominated in summer. The high-ozone weather categories (S-W-N direction, LP and C) accounted for 58.7, 66.5, 79.3, 80.6, 49.0, 38.0 and 27.7% of the time in the months from April to October, respectively. These frequencies were highest in July, June, and May, which probably resulted in the highest monthly averaged regional ozone concentrations. However, due to the influence of monsoon circulation, large amounts of rainfall occurred during July: 73 out of 194 days during the 5 years were rainy in category C, which reduced the ozone levels. Notably, severe ozone pollution in May, especially in the second half of May in 2017, was closely related to abnormally high frequencies under the control of the most polluted synoptic categories (LP and C), accounting for 35.5% in 31 days and 50.0% in 16 days (Table S2). With the development of the Siberian High from August to October, the N-E-S direction and A weather categories occurred frequently, and the monthly averaged ozone concentrations declined.

3.3 Effects of synoptic changes on interannual ozone variability

3.3.1 Effect of weather type intensity on interannual ozone variability

The pressure fields for the 26 synoptic types per year from 2013-2017 (Figs. S8-S9) indicated that every synoptic weather type varied in both frequency and intensity. The intensity of the circulation patterns indicated the differences in the center pressure, the location of the predominant system, the pressure gradient, and the domain-averaged sea level pressure. The correlations between ECII and ΔO_3 (as introduced in Section 2.4) differed in the different circulation types in the various cities. For instance, the strong negative correlation between these two variables for weather type C in ZJK (Fig. 7a) indicated that the low values of min slp were associated with high MDA8 O_3 concentrations.

The number of cities and averaged r values according to the corresponding ECII under each circulation type among the 14 cities are shown in Fig. 7b. Overall, the average absolute value of r was 0.74. For circulation type C, ΔO_3 was strongly correlated with min slp in 9 of the cities, and the average r was -0.81, i.e., a strong negative correlation. A strong negative correlation between ΔO_3 and the pressure

gradient was evident for circulation type N, whereas an opposite pattern occurred for circulation types CSE and CS. The reasons for this difference are as follows. Northerly winds prevailed for circulation type N, and high-pressure gradients indicated strong northerly winds that brought clean air masses from the north, which resulted in a decrease in the MDA8 O_3 concentration. However, high temperatures and RH as well as prevailing southerly or easterly winds (Figs. S3-S5) occurred in southern cities in the CSE and CS circulation types. In addition, the abundance of precursors and ozone in the upwind region facilitated ozone formation and transport with the increasing pressure gradient (wind speeds).

Even under the same weather type controls, the ECII and the values of r differed in the different cities. This phenomenon was caused by differences in geographic location, topographic discrepancies, and the properties of the upwind air mass. Therefore, under the control of the same weather type, the ECII was the same in adjacent cities.

3.3.2 Quantifying the effects of the interannual synoptic changes on the interannual ozone variability

Based on Equations (1) and (2), we reconstructed the interannual ozone levels by taking into account either frequency-only or both frequency and intensity variations in synoptic circulations, which are $\overline{\overline{O_{3m}}}(\mathrm{fre})$ and $\overline{\overline{O_{3m}}}(\mathrm{fre}+\mathrm{int})$, respectively. The differences between the maximum and minimum annual reconstructed ozone are labeled as $\Delta\overline{\overline{O_{3m}}}(\mathrm{fre})$ and $\Delta\overline{\overline{O_{3m}}}(\mathrm{fre}+\mathrm{int})$, respectively. ΔO_3_obs differed between the maximum and minimum for the annual observed O_3 concentration. Thus, the contributions of interannual variability in O_3 influenced by frequency-only and frequency and intensity variations in synoptic circulation were $\Delta\overline{\overline{O_{3m}}}(\mathrm{fre})/\Delta O_3$ _obs and $\Delta\overline{\overline{O_{3m}}}(\mathrm{fre}+\mathrm{int})/\Delta O_3$ _obs, respectively, which indicate the interannual oscillations in ozone levels caused by synoptic variability.

The observed and reconstructed (influenced by frequency-only and frequency and intensity variations in synoptic circulations) interannual MDA8 O_3 levels for 5 years in 14 cities and the whole region are shown in Fig. 8. The contributions of interannual variability in O_3 influenced by frequency and intensity variations in synoptic circulation ranged from 44.1 to 69.8% over the 14 cities, and the contributions by frequency-only variations ranged from 5.2 to 23.4%. Obviously, the interannual fluctuations in the ozone concentration were caused mainly by weather type intensity changes in North China. In addition, based on the regional averaged scale, the interannual variability in the domain-averaged observed MDA8 O_3 in 14 cities varied from averaged maximum values of 135 μg m^{-3} in 2017 to a minimum of 104 μg m^{-3} in 2013. The contributions of variations in circulation patterns to interannual O_3 increases were 39.2%, and the remaining interannual variability was possibly due to nonlinear relationships resulting from recent emission control measures over North China.

In most cities, the contributions of synoptic circulation changes on ozone variability obtained here (44.1-69.8%) are higher than that (50%) estimated by Zhang et al. (2013). The difference could be attributed to our results being based on (1) more weather types, (2) weather types covering all days, and (3) more CIIs, which can better characterize the intensity of slp. Furthermore, a higher contribution in single city and increasing reconstructed ozone indicate that synoptic circulation patterns play an important role in the ozone variability in North China. However, our regional contribution (39.2%) is lower than that (46%) estimated by Hegarty et al. (2007), which reveals that the increasing trend of ozone concentrations from 2013 to 2017 in North China is largely associated with the impact of its precursors.

3.4 Quantifying the impact of weather patterns on day-to-day ozone concentration and forecasting daily ozone concentration

Based on the five weather categories defined in Section 3.2.1, a segmented synoptic-regression analysis approach (introduced in Section 2.5) was established to quantify the impact of weather patterns on the day-to-day ozone concentration and to construct the ozone potential forecast model.

The contributions of local meteorological factors to the day-to-day variations in ozone can be evaluated by the explained variance (R_E^2) calculated from the synoptic-regression-based models (Hien et al., 2002; Wang et al., 2009b). Overall, the predicted versus observed MDA8 O_3 concentrations for the validation data are shown in Fig. 9; the predicted concentrations were obtained by inputting the validation data (the part that was not used to build the model, which was 20% of the total data) into the corresponding model equations for the five weather categories for each city. Local meteorological parameters explained 57-63% and 41-52% of the day-to-day variability in the MDA8 O_3 concentration for the northern cities (except for QHD, 34%) and southern cities (except for ZZ, 20%), respectively.

In addition, the results of segmented synoptic-regression analysis in 14 cities, i.e., the daily MDA8 O_3 potential forecast equations for each category in each city, are shown in Table S3. Table 2 represents the number of cities (14 total) from which the meteorological factors were used in a stepwise regression model under each weather category. The results show that Tmax exhibited a strong positive correlation with ozone; thus, this factor is the primary influencing factor in all categories and all cities, as high temperatures are related to high ozone concentrations in North China. V exhibited a positive correlation with O_3 in the northern part of this region (at the north-south boundary at approximately 38.5°N), which means that southerly flow caused an increase in the ozone concentration. Therefore, as discussed in Section 3.2.2, high temperatures and southerly winds were the main factors that contributed to increased ozone concentrations in North China from a regional perspective. Both RH_lag and RH showed a negative correlation with O_3, and the former had more occurrences and greater weights in the equations than the latter. This phenomenon may exist because RH of approximately 40-50% (Zhao et al., 2019) generates more hydroxyl radicals (OH), facilitating ozone formation, and ozone is stored in the residual layer and transported to the surface the next day via convection and diffusion. In addition, TCC is a key factor.

Three statistical measures (R^2, RMSE, and CV) for the building and validation datasets for the 5 weather categories and the composite model, which integrates the 5 weather categories, in the 14 cities (Table S4) indicates that the potential forecast equations for MDA8 O_3 were acceptable in most cities in most cities. Scatterplots of predicted versus observed MDA8 O_3 concentrations in the composite validation datasets in each city are shown in Fig. 9. For the validation data, the prediction of ozone concentration was obtained by inputting the meteorological factors into the simulated formula for the corresponding weather category in each city; therefore, the composite validation datasets indicated the integrated predicted ozone concentrations for the five categories. The results of validation show that R^2 was higher than 0.50, except for QHD, SJZ and ZZ (0.24-0.47), while CV was lower than 40%, except for TY and ZZ.

The results reveal that most of the validation data are within the acceptable error range, as they are concentrated within the 2:1 and 1:2 ratio lines, and the scatters are distributed evenly around the 1:1 line. For example, the comparison of the observed and predicted ozone in Beijing during our study period is shown in Fig. S10. This finding also indicates that the segmented synoptic-regression approach is practical for constructing ozone potential forecasting models in most cities in North China.

In brief, the aforementioned results can provide references for daily MDA8 O_3 prediction for each city and facilitate the understanding and evaluations of the impact of local meteorology on daily ozone variations on an urban scale.

4 Conclusions

In this study, we demonstrated the interannual/monthly variations in the surface MDA8 O_3 concentration in North China during April-October 2013-2017, investigated the relationship between weather types and MDA8 O_3 levels, quantified the contributions of weather types and local variations in meteorological factors to both the interannual and day-to-day variability in ozone, and built ozone potential forecast equations. The main results are as follows:

1. The annual domain-averaged concentrations of MDA8 O_3 during 2013-2017 were 102, 109, 116, 119, and 136 μg m^{-3}, respectively, and the highest exceedance ratio (31.1%) was observed in 2017. The monthly mean MDA8 O_3 concentrations were 112, 138, 149, 132, 124, 117, and 75 μg m^{-3} from April to October, respectively, with a significantly increasing rate of 0.87 μg m^{-3} $month^{-1}$ during the five-year period. The most polluted cities were concentrated around Beijing, the southeast of Hebei and the west and north of Shandong.

2. Twenty-six weather types were objectively identified based on the Lamb-Jenkinson method and combined into five weather categories according to similar meteorological factors and MDA8 O_3 concentrations. The high ozone levels in 2017 and during May-July were partly due to the high frequency of the highly polluted weather categories (S-W-N direction, LP and C) resulting from high temperatures, moderate RH and southerly air flows.

3. The intensity of synoptic circulation patterns was the dominant factor through which variations in weather types influenced the variability in the ozone levels. The contributions of interannual variability in O_3 influenced by both frequency and intensity variations in synoptic circulation patterns ranged from 44 to 70% over the 14 cities that were evaluated in detail, whereas the contributions of the variations in circulation patterns to the increase in the interannual O_3 from 2013 to 2017 was only 39.2% based on a regionally averaged scale.

4. The results of the daily ozone potential forecast equations in the 14 cities showed that high temperatures, moderate RH and southerly winds could result in severe ozone pollution in the northern part of North China, whereas the southern part was mainly affected by high temperatures and RH. Local meteorological parameters explained 55-64% and 43-49% of the day-to-day MDA8 O_3 variability for the northern cities (except for QHD, 32%) and southern cities (except for ZZ, 25%), respectively.

Author contribution

LL Wang designed this research. JD Liu and LL Wang interpreted the data and wrote the paper. MG Li processed some of the data. The weather type classification program was provided by ZH Liao. Y Sun, T Song, and WK Gao provided some of the $PM_{2.5}$ and O_3 data. Y Li provided some of the meteorological data. All of the authors commented on the paper.

Data availability

The daily average mass concentrations of ozone were obtained from the National Urban Air Quality Real-time Publishing Platform (http://106.37.208.233:20035/) issued by the Chinese Ministry of Ecology and Environment. Daily meteorological data were obtained from the China Meteorological Administration in the Meteorological Information Combine Analysis and Process System (MICAPS), and daily meteorological reanalysis data (gridded at 1°× 1°) were obtained from ERA-Interim (https://apps.ecmwf.int/datasets/data/interim-full-daily/levtype=sfc/). All of the data can be obtained upon request.

Competing interests

The authors declare that they have no conflict of interest.

Acknowledgments

This work was partially supported by grants from the National Key R&D Plan (Quantitative Relationship and Regulation Principle between Regional Oxidation Capacity of Atmospheric and Air Quality 2017YFC0210003), the National Natural Science Foundation of China (No. 41505133 & 41775162), the Strategic Priority Research Program of the Chinese Academy of Sciences (No. XDA19020303), the National Research Program for Key Issues in Air Pollution Control (DQGG0101), the Postgraduate Research & Practice Innovation Program of Jiangsu Province (No. 1344051901061) and a program of the China Scholarships Council. We give special thanks to the National Earth System Science, Data Sharing Infrastructure, and the National Science & Technology Infrastructure of China.

References

Barrero, M. A., Grimalt, J. O., and Cantón, L.: Prediction of daily ozone concentration maxima in the urban atmosphere, Chemometrics and Intelligent Laboratory Systems, 80, 67-76, 10.1016/j.chemolab.2005.07.003, 2006.

Bloomer, B. J., Stehr, J. W., Piety, C. A., Salawitch, R. J., and Dickerson, R. R.: Observed relationships of ozone air pollution with temperature and emissions, Geophysical Research Letters, 36, 269-277, 2009.

Bloomer, B. J., Vinnikov, K. Y., and Dickerson, R. R.: Changes in seasonal and diurnal cycles of ozone and temperature in the eastern U.S, Atmospheric Environment, 44, 2543-2551, 2010.

Chan, C. K., and Yao, X.: Air pollution in mega cities in China, Atmospheric Environment, 42, 1-42, 10.1016/j.atmosenv.2007.09.003, 2008.

Chen, Z. H., Cheng, S. Y., Li, J. B., Guo, X. R., Wang, W. H., and Chen, D. S.: Relationship between atmospheric pollution processes and synoptic pressure patterns in northern China, Atmospheric Environment, 42, 6078-6087, 10.1016/j.atmosenv.2008.03.043, 2008.

Comrie, A. C., and Yarnal, B.: Relationships between synoptic-scale atmospheric circulation and ozone concentrations in Metropolitan Pittsburgh, Pennsylvania, Atmospheric Environment.part B.urban Atmosphere, 26, 301-312, 1992.

Conway, D., and Jones, P. D.: The use of weather types and air flow indices for GCM downscaling, Journal of Hydrology, 212-213, 348-361, https://doi.org/10.1016/S0022-1694(98)00216-9, 1998.

Cooper, O. R., Moody, J. L., Parrish, D. D., Trainer, M., Ryerson, T. B., Holloway, J. S., Hübler, G., Fehsenfeld, F. C., Oltmans, S. J., and Evans, M. J.: Trace gas signatures of the airstreams within North Atlantic cyclones: Case studies from the North Atlantic Regional Experiment (NARE '97) aircraft intensive, Journal of Geophysical Research: Atmospheres, 106, 5437-5456, 10.1029/2000jd900574, 2001.

Cooper, O. R., Moody, J. L., Parrish, D. D., Trainer, M., Holloway, J. S., Hübler, G., Fehsenfeld, F. C., and Stohl, A.: Trace gas composition of midlatitude cyclones over the western North Atlantic Ocean: A seasonal comparison of O3 and CO, Journal of Geophysical Research: Atmospheres, 107, ACH 2-1-ACH 2-12, 10.1029/2001jd000902, 2002.

Delcloo, A. W. a. D. B., H.: Five day 3D back trajectory clusters and trends analysis of the Uccle ozone sounding time series in the lower troposphere (1969–2001), Atmos. Environ., 42, 4419–4432, 2008.

Demuzere, M., Trigo, R. M., Vila-Guerau de Arellano, J., and van Lipzig, N. P. M.: The impact of weather and atmospheric circulation on O3 and PM10 levels at a rural mid-latitude site, Atmos. Chem. Phys., 9, 2695-2714, https://doi.org/10.5194/acp-9-2695-2009, 2009.

Demuzere, M., and van Lipzig, N. P. M.: A new method to estimate air-quality levels using a synoptic-regression approach. Part I: Present-day O3 and PM10 analysis, Atmospheric Environment, 44, 1341-1355, https://doi.org/10.1016/j.atmosenv.2009.06.029, 2010.

Eder, B. K., Davis, J. M., and Bloomfield, P.: An Automated Classification Scheme Designed to Better Elucidate the Dependence of Ozone on Meteorology, J.appl.meteor, 33, 1182-1199, 1994.

Fleming, Z. L., Doherty, R. M., Von Schneidemesser, E., Malley, C. S., Cooper, O. R., Pinto, J. P., Colette, A., Xu, X., Simpson, D., Schultz, M. G., Lefohn, A. S., Hamad, S., Moolla, R., Solberg, S., and Feng, Z.: Tropospheric Ozone Assessment Report: Present-day ozone distribution and trends relevant to human health, Elem Sci Anth, 6, 12, 10.1525/elementa.273, 2018.

He, J., Yu, Y., Xie, Y., Mao, H., Wu, L., Liu, N., and Zhao, S.: Numerical Model-Based Artificial Neural Network Model and Its Application for Quantifying Impact Factors of Urban Air Quality, Water, Air, & Soil Pollution, 227, 10.1007/s11270-016-2930-z, 2016.

He, J., Gong, S., Yu, Y., Yu, L., Wu, L., Mao, H., Song, C., Zhao, S., Liu, H., Li, X., and Li, R.: Air pollution characteristics and their relation to meteorological conditions during 2014-2015 in major Chinese cities, Environmental pollution, 223, 484-496, 10.1016/j.envpol.2017.01.050, 2017.

Hegarty, J., Mao, H., and Talbot, R.: Synoptic controls on summertime surface ozone in the northeastern United States, Journal of Geophysical Research, 112, 10.1029/2006jd008170, 2007.

Hien, P. D., Bac, V. T., Tham, H. C., Nhan, D. D., and Vinh, L. D.: Influence of meteorological conditions on PM2.5 and PM2.5-10 concentrations during the monsoon season in Hanoi, Vietnam, Atmospheric Environment, 36, 3473-3484, 10.1016/s1352-2310(02)00295-9, 2002.

Jacob, D. J., and Winner, D. A.: Effect of climate change on air quality, Atmospheric Environment, 43, 51-63, 10.1016/j.atmosenv.2008.09.051, 2009.

Kinney, P. L.: Climate change, air quality, and human health, American journal of preventive medicine, 35, 459-467, 10.1016/j.amepre.2008.08.025, 2008.

Lamb, H.: British Isles weather types and a register of the daily sequence of circulation patterns, Geophys. Mem, 116, 1861-1971, 1972.

Li, K., Jacob, D. J., Liao, H., Shen, L., Zhang, Q., and Bates, K. H.: Anthropogenic drivers of 2013–2017 trends in summer surface ozone in China, Proceedings of the National Academy of Sciences, 116, 422-427, 10.1073/pnas.1812168116, 2019.

Liao, Z., Gao, M., Sun, J., and Fan, S.: The impact of synoptic circulation on air quality and pollution-related human health in the Yangtze River Delta region, The Science of the total environment, 607-608, 838-846, 10.1016/j.scitotenv.2017.07.031, 2017.

Liu, Y., Franklin, M., Kahn, R., and Koutrakis, P.: Using aerosol optical thickness to predict ground-level PM2.5 concentrations in the St. Louis area: A comparison between MISR and MODIS, Remote Sens. Environ., 107, 33-44, 10.1016/j.rse.2006.05.022, 2007.

Liu, Y., He, K. B., Li, S. S., Wang, Z. X., Christiani, D. C., and Koutrakis, P.: A statistical model to evaluate the effectiveness of PM2.5 emissions control during the Beijing 2008 Olympic Games, Environ. Int., 44, 100-105, 10.1016/j.envint.2012.02.003, 2012.

Lu, X., Hong, J., Zhang, L., Cooper, O. R., and Zhang, Y.: Severe Surface Ozone Pollution in China: A Global Perspective, Environmental Science & Technology Letters, 5, acs.estlett.8b00366-, 2018.

Lu, X., Zhang, L., Chen, Y., Zhou, M., Zheng, B., Ke, L., Liu, Y., Lin, J., Fu, T.-M., and Zhang, Q.: Exploring 2016–2017 surface ozone pollution over China: source contributions and meteorological influences, Atmospheric Chemistry and Physics, 19, 8339-8361, 10.5194/acp-19-8339-2019, 2019.

Mckendry, I. G., Stahl, K., and Moore, R. D.: Synoptic sea-level pressure patterns generated by a general circulation model: comparison with types derived from NCEP/NCAR re-analysis and implications for downscaling, International Journal of Climatology, 26, 1727-1736, 2006.

Mills, G., Pleijel, H., Malley, C. S., Sinha, B., Cooper, O. R., Schultz, M. G., Neufeld, H. S., Simpson, D., Sharps, K., Feng, Z., Gerosa, G., Harmens, H., Kobayashi, K., Saxena, P., Paoletti, E., Sinha, V., and Xu, X.: Tropospheric Ozone Assessment Report: Present-day tropospheric ozone distribution and trends relevant to vegetation, Elem Sci Anth, 6, 47, 10.1525/elementa.302, 2018.

Monks, P. S., Granier, C., Fuzzi, S., Stohl, A., Williams, M. L., Akimoto, H., Amann, M., Baklanov, A., Baltensperger, U., Bey, I., Blake, N., Blake, R. S., Carslaw, K., Cooper, O. R., Dentener, F., Fowler, D., Fragkou, E., Frost, G. J., Generoso, S., Ginoux, P., Grewe, V., Guenther, A., Hansson, H. C., Henne, S., Hjorth, J., Hofzumahaus, A., Huntrieser, H., Isaksen, I. S. A., Jenkin, M. E., Kaiser, J., Kanakidou, M., Klimont, Z., Kulmala, M., Laj, P., Lawrence, M. G., Lee, J. D., Liousse, C., Maione, M., McFiggans, G., Metzger, A., Mieville, A., Moussiopoulos, N., Orlando, J. J., O'Dowd, C. D., Palmer, P. I., Parrish, D. D., Petzold, A., Platt, U., Pöschl, U., Prévôt, A. S. H., Reeves, C. E., Reimann, S., Rudich, Y., Sellegri, K., Steinbrecher, R., Simpson, D., ten Brink, H., Theloke, J., van der Werf, G. R., Vautard, R., Vestreng, V., Vlachokostas, C., and von Glasow, R.: Atmospheric composition change – global and regional air quality, Atmospheric Environment, 43, 5268-5350, https://doi.org/10.1016/j.atmosenv.2009.08.021, 2009.

Monks, P. S., Archibald, A. T., Colette, A., Cooper, O., Coyle, M., Derwent, R., Fowler, D., Granier, C., Law, K. S., Mills, G. E., Stevenson, D. S., Tarasova, O., Thouret, V., Schneidemesser, E. v., Sommariva, R., Wild, O., and Williams, M. L.: Tropospheric ozone and its precursors from the urban to the global scale from air quality to short-lived climate forcer, Atmospheric Chemistry and Physics, 15, 8889-8973, 10.5194/acp-15-8889-2015, 2015.

Moody, J. L., Munger, J. W., Goldstein, A. H., Jacob, D. J., and Wofsy, S. C.: Harvard Forest regional-scale air mass composition by Patterns in Atmospheric Transport History (PATH), Journal of Geophysical Research: Atmospheres, 103, 13181-13194, 10.1029/98jd00526, 1998.

Pope, R. J., Butt, E. W., Chipperfield, M. P., Doherty, R. M., Fenech, S., Schmidt, A., Arnold, S. R., and Savage, N. H.: The impact of synoptic weather on UK surface ozone and implications for premature mortality, Environmental Research Letters, 11, 124004, 10.1088/1748-9326/11/12/124004, 2016.

569 Pusede, S. E., Steiner, A. L., and Cohen, R. C.: Temperature and Recent Trends in the Chemistry of
570 Continental Surface Ozone, Chemical Reviews, 115, 3898-3918, 10.1021/cr5006815, 2015.
571 Robeson, S. M., and Steyn, D. G.: Evaluation and comparison of statistical forecast models for daily
572 maximum ozone concentrations, Atmospheric Environment Part B Urban Atmosphere, 24, 303-312,
573 1990.
574 Russo, A., Trigo, R. M., Martins, H., and Mendes, M. T.: NO2, PM10 and O3 urban concentrations and
575 its association with circulation weather types in Portugal, Atmospheric Environment, 89, 768-785,
576 10.1016/j.atmosenv.2014.02.010, 2014.
577 Santurtún, A., González-Hidalgo, J. C., Sanchez-Lorenzo, A., and Zarrabeitia, M. T.: Surface ozone
578 concentration trends and its relationship with weather types in Spain (2001–2010), Atmospheric
579 Environment, 101, 10-22, 2015.
580 Shen, L., Mickley, L. J., and Tai, A. P. K.: Influence of synoptic patterns on surface ozone variability
581 over the eastern United States from 1980 to 2012, Atmospheric Chemistry and Physics, 15, 10925-10938,
582 10.5194/acp-15-10925-2015, 2015.
583 Stohl, A., and Trickl, T.: A textbook example of long-range transport: Simultaneous observation of
584 ozone maxima of stratospheric and North American origin in the free troposphere over Europe, Journal
585 of Geophysical Research Atmospheres, 104, 30445-30462, 1999.
586 Tang, G., Wang, Y., Li, X., Ji, D., Hsu, S., and Gao, X.: Spatial-temporal variations in surface ozone in
587 Northern China as observed during 2009–2010 and possible implications for future air quality control
588 strategies, Atmospheric Chemistry and Physics, 12, 2757-2776, 10.5194/acp-12-2757-2012, 2012.
589 Trigo, R. M., and Dacamara, C. C.: Circulation weather types and their influence on the precipitation
590 regime in Portugal, International Journal of Climatology, 20, 1559-1581, 2000.
591 Verstraeten, W. W., Neu, J. L., Williams, J. E., Bowman, K. W., Worden, J. R., and Boersma, K. F.:
592 Rapid increases in tropospheric ozone production and export from China, Nature Geoscience, 8, 690,
593 10.1038/ngeo2493, 2015.
594 Wang, T., Wei, X., Ding, A., Poon, S. C., Lam, K., Li, Y., Chan, L., and Anson, M.: Increasing surface
595 ozone concentrations in the background atmosphere of Southern China, 1994-2007, Atmospheric
596 Chemistry and Physics, 2009a.
597 Wang, W. T., Primbs, T., Tao, S., and Simonich, S. L. M.: Atmospheric Particulate Matter Pollution
598 during the 2008 Beijing Olympics, Environmental Science & Technology, 43, 5314-5320,
599 10.1021/es9007504, 2009b.
600 Wang, Y., Hao, J., McElroy, M. B., Munger, J. W., Ma, H., Chen, D., and Nielsen, C. P.: Ozone air
601 quality during the 2008 Beijing Olympics: effectiveness of emission restrictions, Atmospheric Chemistry
602 and Physics, 9, 5237-5251, DOI 10.5194/acp-9-5237-2009, 2009c.
603 Yarnal, B.: Synoptic Climatology in Environmental Analysis A Primer, Journal of Preventive Medicine
604 Information, 347, 170-180, 1993.
605 Zhang, J. P., Zhu, T., Zhang, Q. H., Li, C. C., Shu, H. L., Ying, Y., Dai, Z. P., Wang, X., Liu, X. Y.,
606 Liang, A. M., Shen, H. X., and Yi, B. Q.: The impact of circulation patterns on regional transport
607 pathways and air quality over Beijing and its surroundings, Atmospheric Chemistry and Physics, 12,
608 5031-5053, 10.5194/acp-12-5031-2012, 2012.
609 Zhang, Y., Mao, H., Ding, A., Zhou, D., and Fu, C.: Impact of synoptic weather patterns on spatio-
610 temporal variation in surface O3 levels in Hong Kong during 1999–2011, Atmospheric Environment, 73,
611 41-50, 10.1016/j.atmosenv.2013.02.047, 2013.

Zhao, W., Tang, G., Yu, H., Yang, Y., Wang, Y., Wang, L., An, J., Gao, W., Hu, B., Cheng, M., An, X., Li, X., and Wang, Y.: Evolution of boundary layer ozone in Shijiazhuang, a suburban site on the North China Plain, Journal of Environmental Sciences, 83, 152-160, https://doi.org/10.1016/j.jes.2019.02.016, 2019.

Tables

Table 1. Weather types, ozone concentrations and meteorological conditions for 5 weather categories.

category	type	ozone	fre	Tmax	RH	rain	TCC	ws	BLH	div	v-v	characteristics
N-E-S direction	N	108	5.4	25.9	64.5	2.2	6	2.1	749	0.85	2.28	MDA8 O_3 (98±6 μg m^{-3}). Cool, moderate rain, moderate TCC, and low BLH, predominant wind directions are north and east, clean air masses from inner Mongolia or the eastern ocean.
	NE	94	6.4	25.5	72.1	5.0	7	2.2	637	-1.01	-0.70	
	E	98	4.7	25.4	70.5	3.4	6	2.1	618	-1.34	-1.85	
	SE	105	2.3	22.8	71.5	4.9	7	2.4	612	-1.25	-3.85	
	AN	101	1.7	22.2	61.2	1.5	5	2.3	738	2.36	5.12	
	ANE	88	2.4	23.1	67.9	2.3	6	2.2	681	0.79	1.53	
	AE	94	1.3	23.2	65.8	2.2	7	2.3	618	-0.10	0.12	
	ASE	99	1.1	22.4	71.3	2.3	7	2.2	578	1.10	0.03	
S-W-N direction	S	112	4.1	25.4	65.7	2.2	6	2.2	642	0.28	-1.23	MDA8 O_3 (122±8 μg m^{-3}). Moderate T and BLH, lower RH, weak wind, sporadic clouds and precipitation, divergence in low troposphere. Prevailing southerly and westerly winds.
	SW	131	6.2	26.5	60.3	0.6	5	2.1	716	1.81	1.34	
	W	133	5.4	26.6	58.3	1.0	5	2.2	763	2.33	2.43	
	NW	124	4.2	26.8	58.7	1.6	6	2.3	835	1.66	3.45	
	AS	120	1.4	24.8	63.3	0.7	6	2.0	641	1.76	0.54	
	AS	114	2.6	24.5	62.2	0.7	6	1.9	666	2.53	1.02	
	AW	126	1.0	23.8	58.5	0.2	5	1.8	685	3.14	4.16	
	AN	115	1.5	23.4	55.2	0.9	6	2.3	794	2.47	5.07	
LP	CN	135	2.0	29.8	68.0	2.2	6	1.9	732	0.09	0.92	The hybrid of cyclone and direction types, MDA8 O_3 (126±16 μg m^{-3}). Widespread hot, humid, a small amount of clouds and rain, comparatively high BLH.
	CNE	119	1.8	28.2	66.0	3.2	6	2.2	724	-1.15	-0.19	
	CE	109	0.8	25.4	73.6	6.4	7	2.1	559	-2.67	-3.65	
	CSE	103	0.7	25.1	62.6	1.4	6	2.6	725	-1.65	-0.58	
	CS	123	1.0	27.4	65.7	1.6	5	2.1	693	-0.40	-0.67	
	CS	155	2.2	29.4	62.6	1.2	5	2.3	796	0.96	0.58	
	CW	140	2.6	28.6	62.3	1.3	5	2.2	778	0.95	0.93	
	CN	124	1.5	29.2	62.4	4.5	6	2.5	853	0.12	1.26	
C		128	18.1	29.5	67.1	3.8	6	2.2	715	-1.20	-1.22	Cyclone, similar to LP.
A		96	17.5	22.3	64.5	1.5	6	2.0	632	2.54	2.66	Anticyclone, similar to N-E-S direction.

Note: Ozone, MDA8 O_3 concentration (μg m^{-3}); fre, frequency of each type (%); Tmax, daily maximum temperature (℃); RH, relative humidity (%); rain, total daily precipitation (mm); TCC, total cloud cover; WS, wind speed (m s^{-1}); BLH, boundary layer height (m); div, divergence of the wind field (10^{-6} s^{-1}) from 1000 to 850 hPa (7 levels); and v-v, vertical velocity from 1000 to 100 hPa (10^{-2} Pa s^{-1}).

Table 2 All parameters used in the stepwise regression and the number of cities (out of 14) for which each variable was selected for each weather category.

factors	N-E-S direction	S-W-N direction	LP	C	A
RH (%)	2	4	3	4	6
Tmax (°C)	14	14	14	14	14
rain (mm)	0	2	2	0	2
U	2	3	3	3	1
V	9	6	6	7	2
wd (°)	2	0	0	1	1
ws (m s^{-1})	4	1	1	0	2
pre (hPa)	0	0	0	0	0
RH_lag (%)	11	5	5	4	4
Tmax_lag (°C)	3	0	0	1	0
rain_lag(mm)	1	0	0	0	0
U_lag	2	1	1	1	1
V_lag	4	0	0	0	4
wd_lag (°)	0	0	0	0	0
ws_lag (m s^{-1})	1	3	3	1	4
pre_lag (hPa)	1	0	0	1	1

Note: RH, Tmax, rain, U, V, wd, ws and pre are relative humidity, maximum temperature, precipitation, u component, v component, wind direction, wind speed and pressure, respectively. The suffix 'lag' means the meteorological factors from the previous day.

629 **Figures**

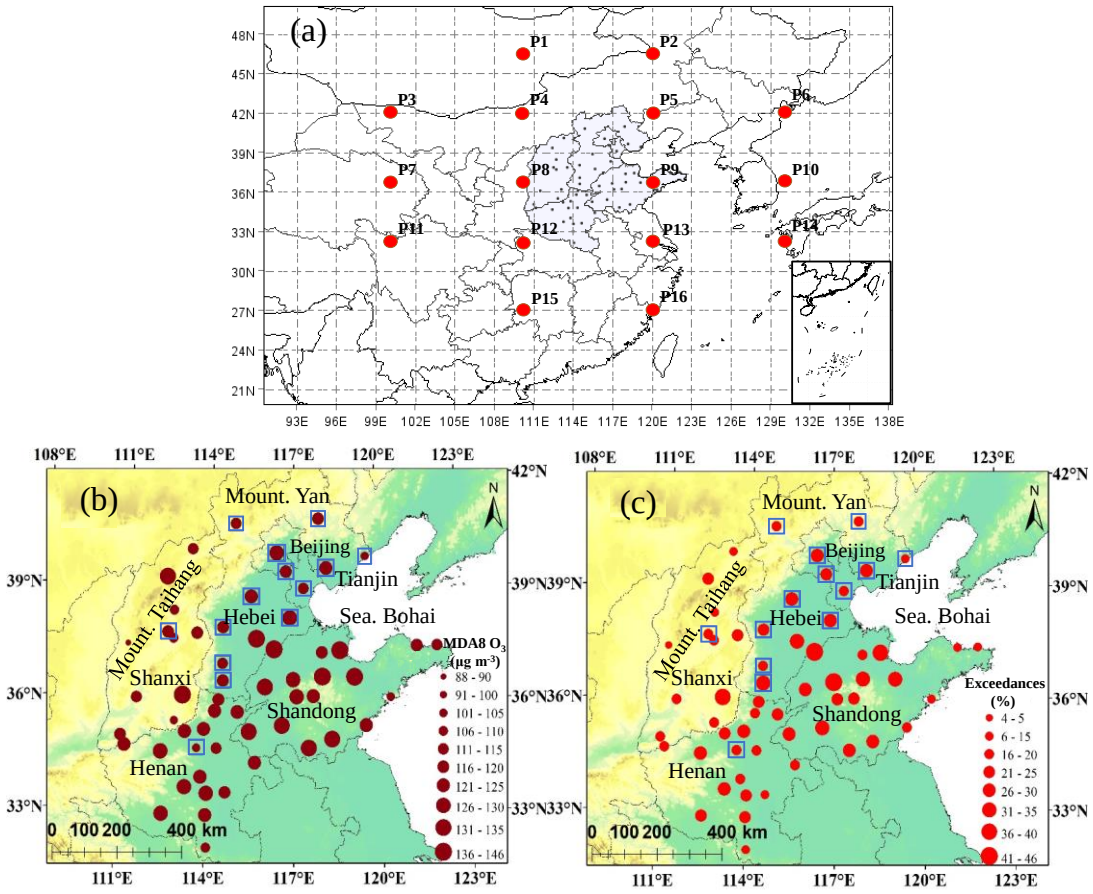

630

631 **Fig. 1. Location of North China (shaded area), all cities (black dots) and sea level pressure grids (a). The 16**
632 **red points show the locations of the 5°×10° mean sea level pressure grids used for the Lamb-Jenkinson**
633 **weather type classification. The spatial distributions of the maximum daily 8-h running average O_3 (MDA8**
634 **O_3) concentration (b) and exceedance ratios (c) for 58 cities. Statistics for 2013-2017 are shown in blue boxes;**
635 **the other boxes are those for 2015-2017. The base map is topography; the elevations of the Taihang Mountains**
636 **are more than 1200 meters, and the Yan Mountains range from 600 to 1500 meters.**

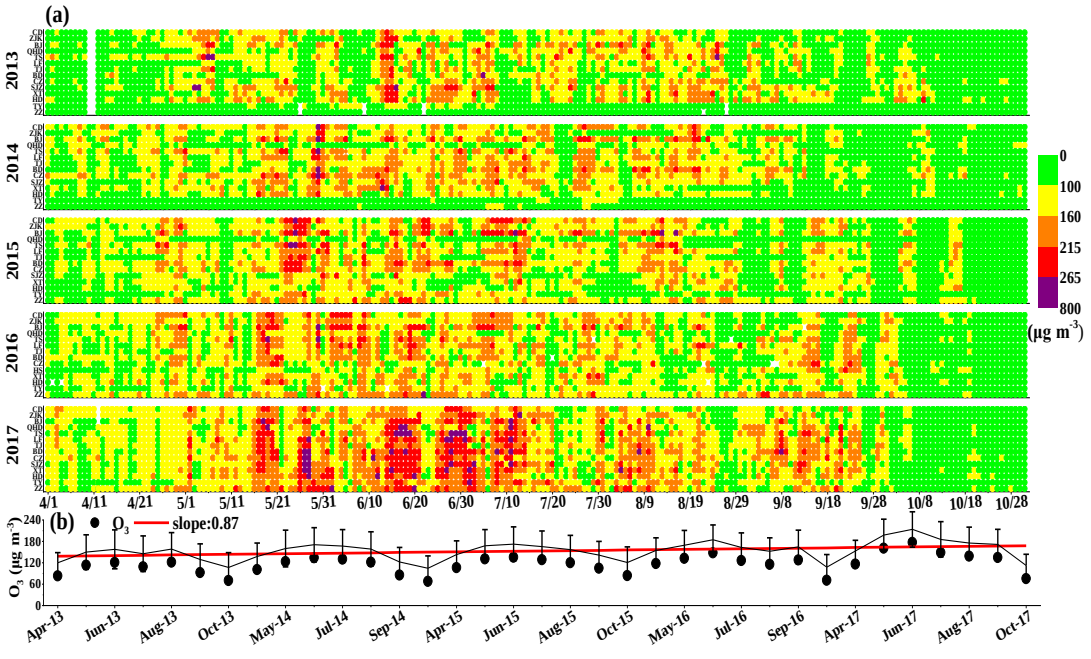

Fig. 2. Time series of daily MDA8 O_3 concentrations in 14 cities (north to south) (a), together with monthly averaged concentrations and standard deviations (b), during April to October from 2013 to 2017. Five ranks represent different air-quality levels, including excellent (green spots), good (yellow), lightly polluted (orange), moderately polluted (red) and heavily polluted (purple) days with cut-off concentrations of 100, 160, 215, and 265 μg m^{-3}, respectively. The fit line (red line) in (b) represents the increasing trend of monthly mean MDA8 O_3.

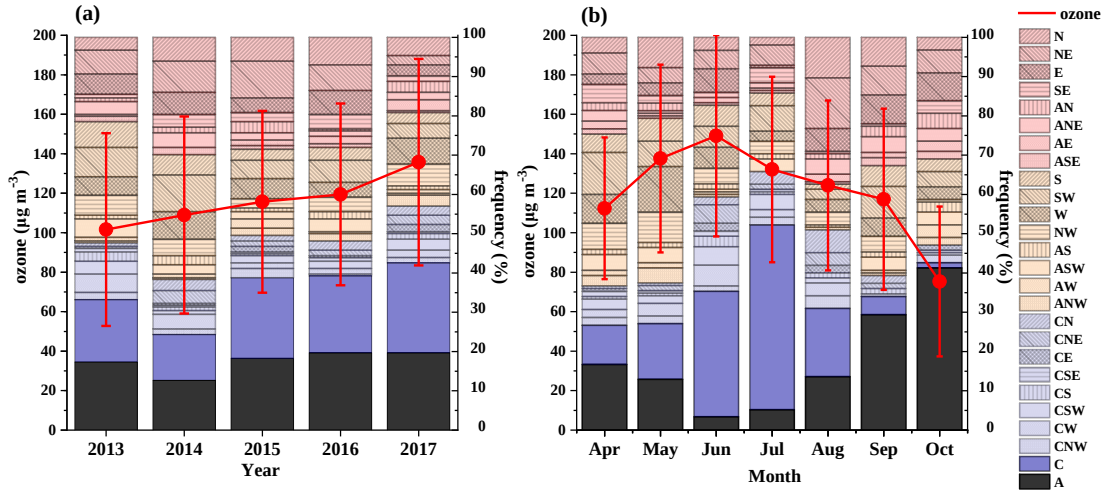

Fig. 3. Interannual (a) and monthly (b) averaged concentrations of ozone and frequencies of 26 weather types from April-October 2013-2017. The red dots represent the mean values, the vertical red lines indicate the standard deviations, and stacked charts represent the percentages of various weather types (2013 and 2014 are averaged for 14 cities; 2015-2017 are averaged for 58 cities). The pink, orange, light blue, dark blue and black areas represent the weather categories N-E-S direction, S-W-N direction, LP, C and A, respectively.

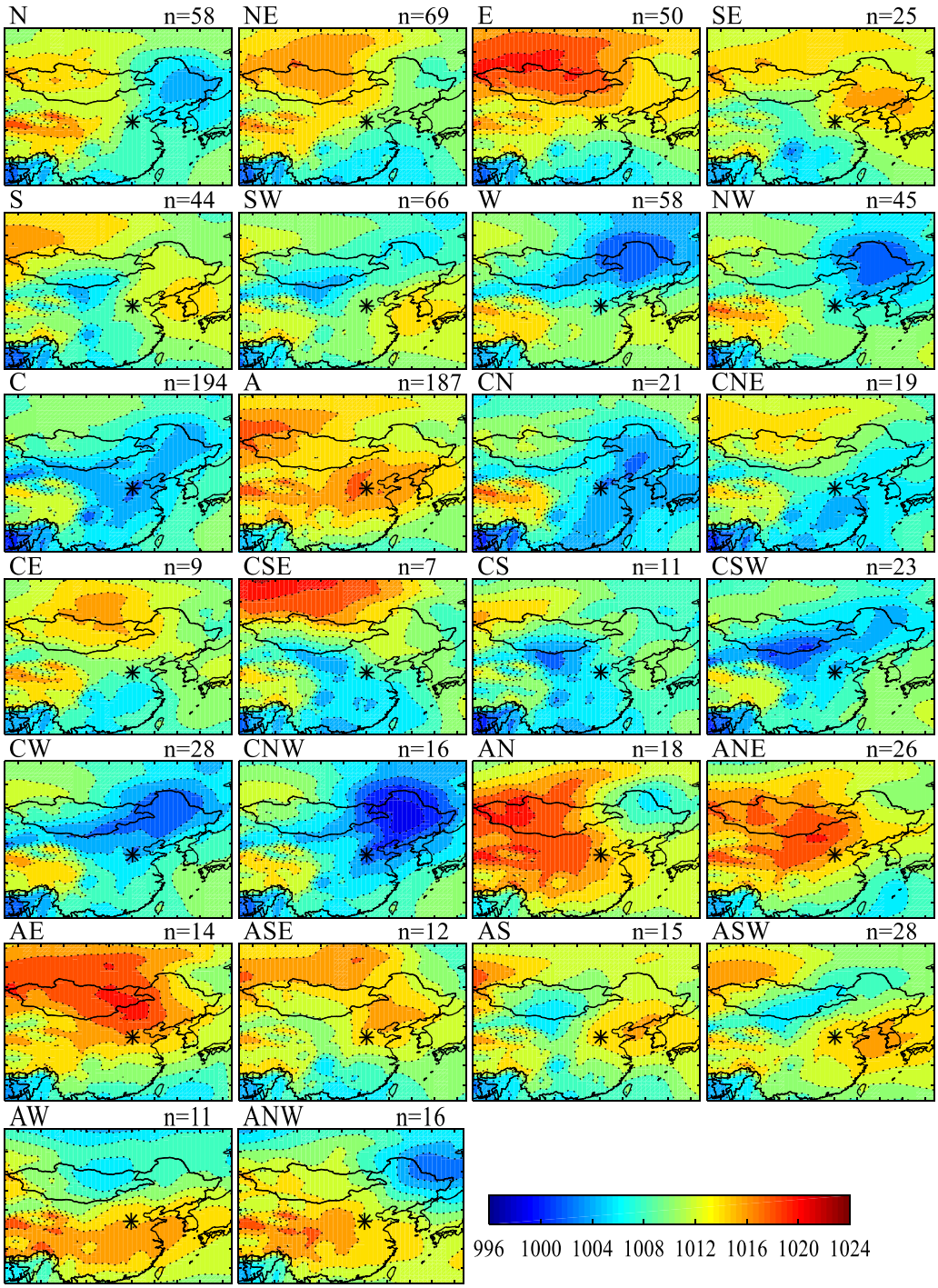

Fig. 4. Mean surface pressure field (unit: hPa) for the 26 weather types during April-October of 2013-2017 and occurrence days (1070 days in total). '*' indicates the center of North China.

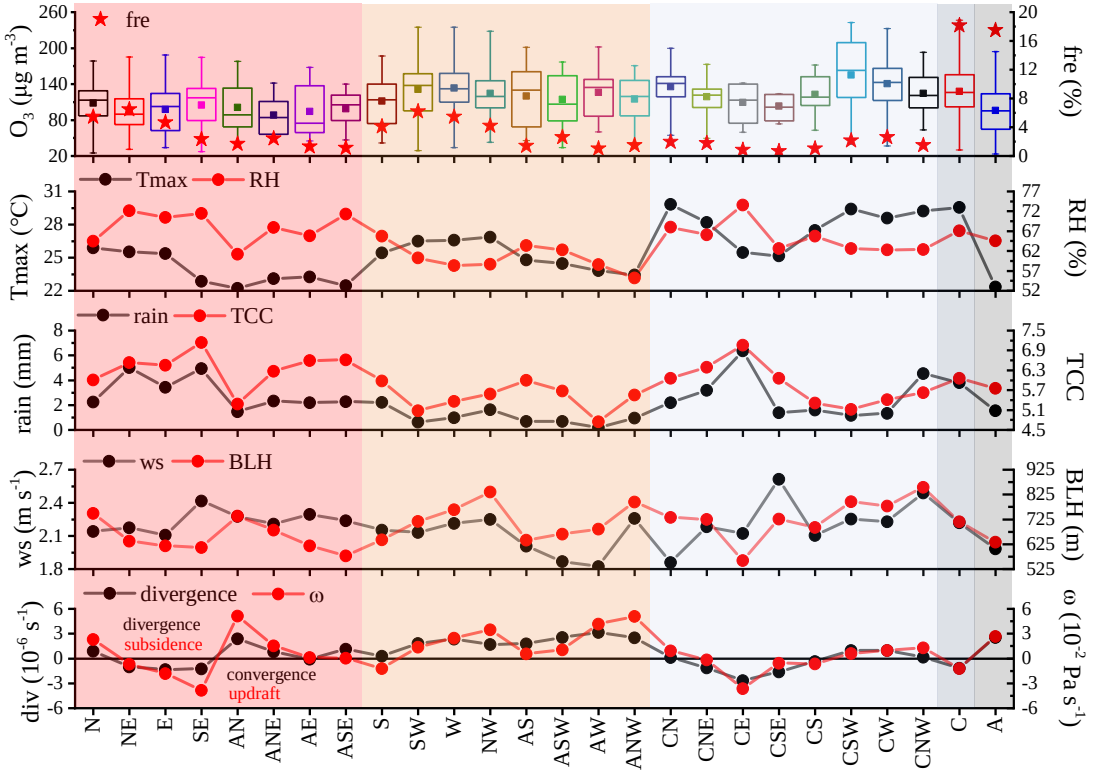

Fig. 5. Box chart of domain-averaged MDA8 O_3 concentrations, occurrence frequency of weather types (fre), and mean values of meteorological factors in 26 weather types during April-October 2013-2017. In the box chart, the solid square indicates the mean, the horizontal lines across the box are the averages of the first, median, and third quartiles, respectively, and the lower and upper whiskers represent the 5th and 95th percentiles, respectively. The pink, orange, light blue, dark blue and black areas represent the weather categories N-E-S direction, S-W-N direction, LP (low-pressure related weather patterns), C (cyclone) and A (anticyclone), respectively.

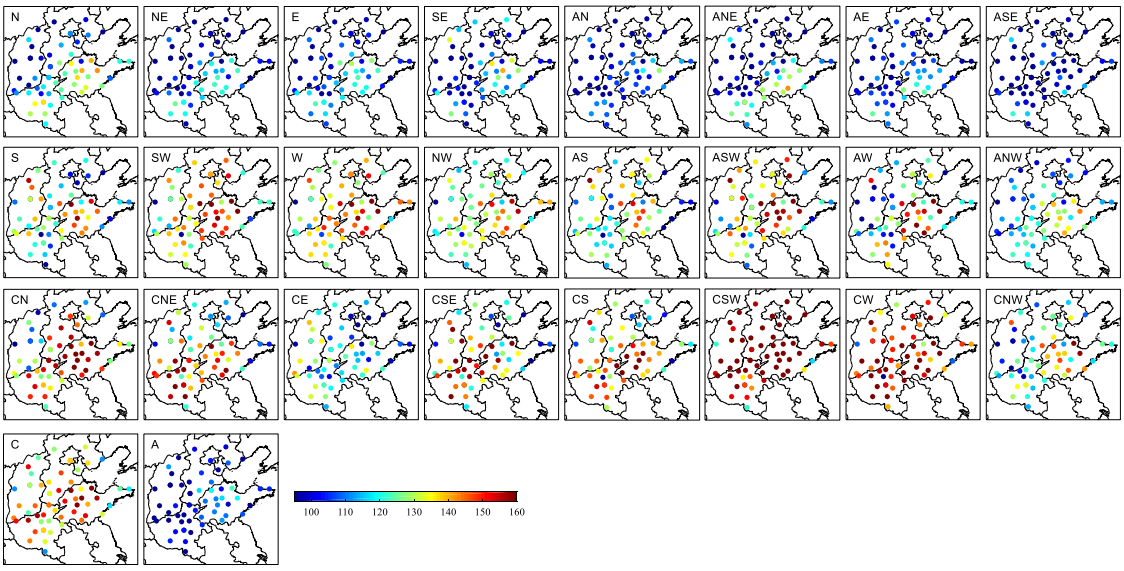

Fig. 6. Spatial distribution of average MDA8 O_3 for the 26 weather types. The first, second, and third rows correspond to the weather categories N-E-S direction, S-W-N direction and LP, respectively, and the fourth row includes both categories C and A.

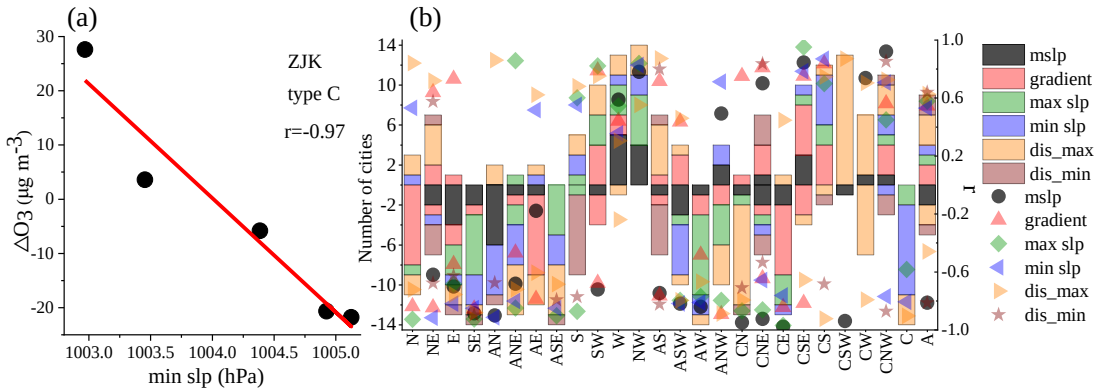

Fig. 7. Scatterplot of ΔO_3 versus min slp for weather type C in ZJK (a). The red line represents the linear fitting between min slp (the ECII under weather type C in ZJK) and ΔO_3 (the difference between the MDA8 O_3 for a given year and the corresponding 5-year average); r represents the correlation coefficient. The number of cities (histogram) and averaged correlation coefficient r (points of different shapes) according to corresponding ECII under each weather type among 14 cities (b). The number of cities with positive/negative values represents positive/negative correlations between ECII and ΔO_3. For example, under CW controls, there are 1, 6 and 7 cities where ECII corresponds to mslp with a positive correlation, dis max with a positive correlation, and dis max with a negative correlation, respectively, and the average r is 0.74 and 0.70 and -0.79, respectively.

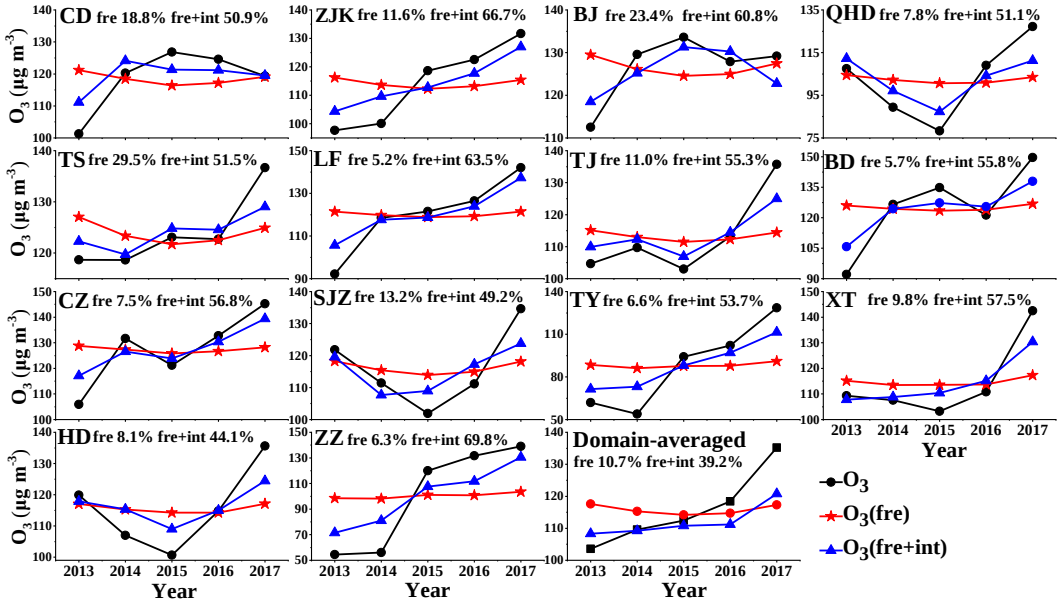

Fig. 8. The interannual MDA8 O_3 concentration trends for observed and reconstructed O_3 based on variations in weather types in 14 cities. The black lines represent the observed interannual MDA8 O_3 trend, whereas the red and blue lines are the trends of reconstructed MDA8 O_3 concentrations according to the frequency-only and both frequency and intensity of weather types changes, respectively. The percentages in each city indicate the O_3 interannual variabilities influenced by frequency-only and by both frequency and intensity of weather type changes.

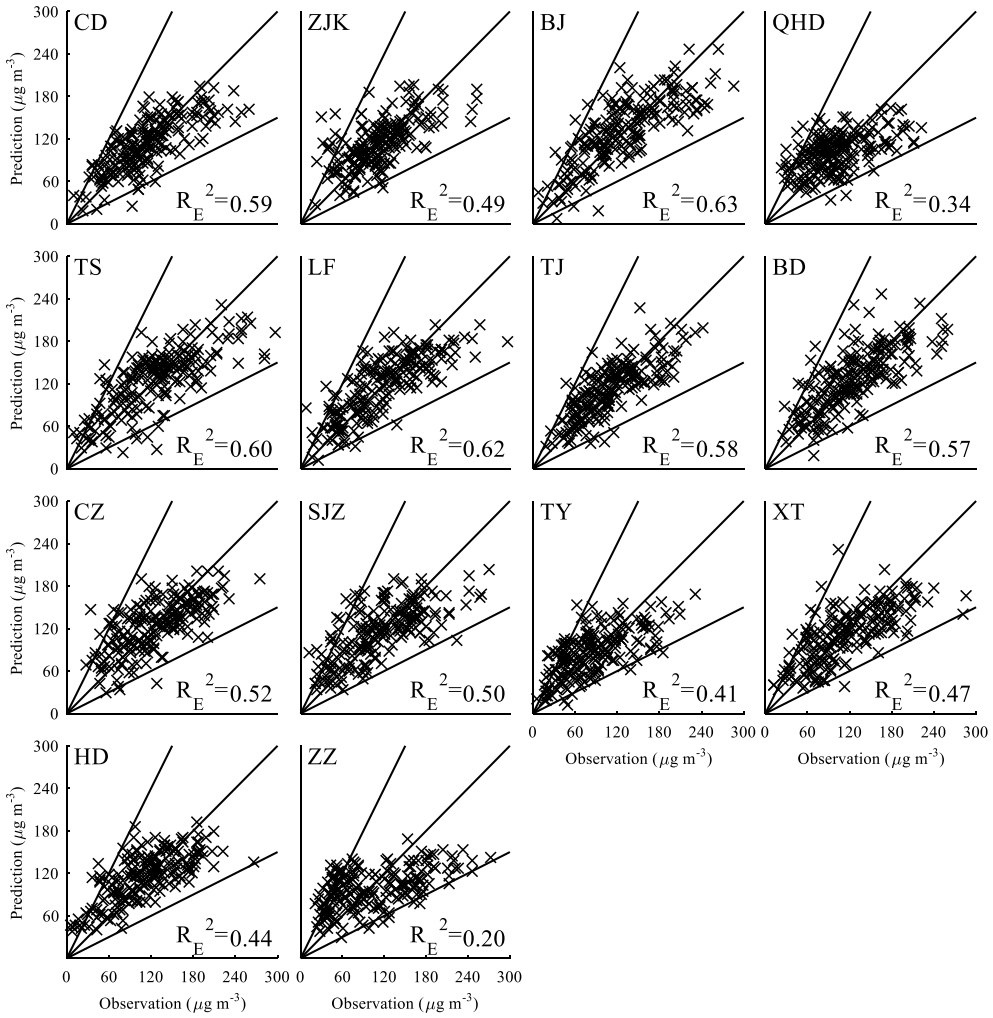

685

686 **Fig. 9. Scatter plots of predicted versus observed MDA8 O_3 concentrations for each city. The predicted**
687 **concentrations were obtained by inputting the validation data (20% of the total data) into the corresponding**
688 **model equations for five weather categories. The R_E^2 values indicate the percentage of explained variance in**
689 **the composite model that contains the building and validation datasets for each city. The three black lines**
690 **indicate 2:1, 1:1 and 1:2 ratio lines of predictions and observations.**